GMR
The Original

ASSESSMENT OF CARBON DIOXIDE SEQUESTRATION POTENTIAL OF SELECTED TREE SPECIES IN BHARATHIDASAN UNIVERSITY MAIN CAMPUS THROUGH PHYSIOLOGICAL AND BIOCHEMICAL PROFILING MECHANISMS

A.K. Arun Prasath[1], M. Govindaraju[2*], P. Edison Raj Godwin[3], Anantha Narayanan Sri Gayathri[4]

[1,2,3,4] Centre for Climate Change Research (CCCR), Department of Environmental Biotechnology, Bharathidasan University, Tiruchirappalli 620024, Tamil Nadu, India
*Corresponding Author: M. Govindaraju, mgrasu@bdu.ac.in

ABSTRACT

Selecting tree species for institutional and urban afforestation programs across semi-arid South Asia has traditionally relied on historical preferences or aesthetic criteria, without biochemical validation of interspecific carbon fixation capacity. This study establishes a unified structural-metabolic profile by quantifying five core carbon-processing enzymes alongside leaf-level gas exchange parameters and allometric biomass partitioning across ten co-occurring tropical tree species (Acacia nilotica, Pithecellobium dulce, Couroupita guianensis, Butea monosperma, Sapindus emarginatus, Neolamarckia cadamba, Gmelina arborea, Prosopis cineraria, Dalbergia latifolia and Cassia roxburghii) under identical peak-summer microclimatic field conditions at Bharathidasan University campus, Tiruchirappalli, Tamil Nadu, India. The results reveal a clear metabolic hierarchy wherein upstream enzymatic efficiency directly limits downstream stomatal gas transport and long-term structural carbon storage. Prosopis cineraria emerged as the most efficient carbon sink, displaying the highest carbonic anhydrase (CA) activity (8.95×10^{-8} U mg^{-1} protein), the most responsive Rubisco activation (lowest residual absorbance: 0.81 at 340 nm), and elevated photorespiratory protection via glycolate oxidase (1.32 µmol mg^{-1} protein min^{-1}) and catalase (1.42 µmol mg^{-1} protein min^{-1}). This superior kinetic throughput supported a net photosynthetic rate (Pn = 19.2 µmol CO_2 m^{-2} s^{-1}) and a total individual biomass accumulation of ~14,960 kg (~25,804 kg CO_2 eq). A multi-trait Carbon Sequestration Index (CSI) stratified the ten species into three distinct afforestation tiers, providing an empirical, biochemically-validated framework for selecting high-performance tree species for regional climate management initiatives under India's 2030 Nationally Determined Contribution (NDC) targets.

KEYWORDS: Enzyme kinetics, Carbon sequestration, Semi-arid afforestation, Gas exchange physiology, Allometric biomass, Carbonic anhydrase, Rubisco, RT-qPCR, Carbon Sequestration Index, Tropical trees.

GRAPHICAL ABSTRACT

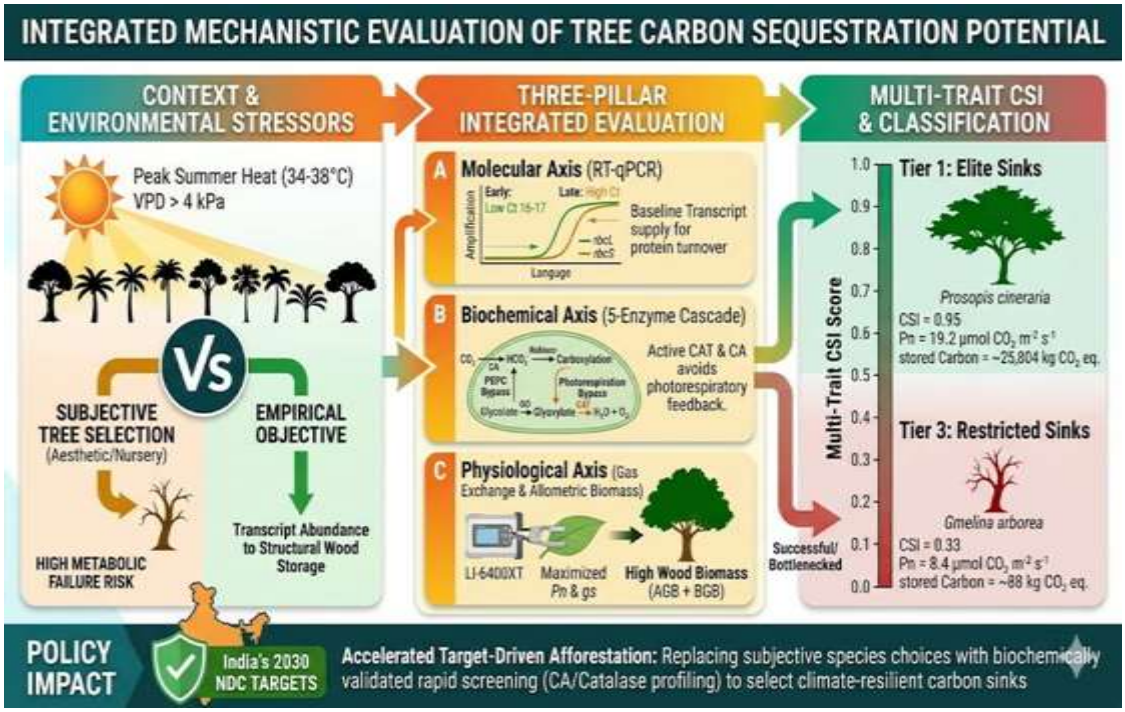

1. INTRODUCTION

Anthropogenic emissions have elevated atmospheric carbon dioxide (CO_2) concentrations beyond 425 ppm, intensifying global thermal anomalies and disrupting regional hydrological cycles.[1,2] The Global Carbon Budget 2023 confirmed that terrestrial ecosystems absorbed approximately 3.1 ± 0.6 GtC per year over the past decade, yet this biological drawdown remains insufficient to offset fossil fuel emissions of ~10.0 GtC yr-1.[3] Biological mitigation through targeted afforestation remains one of the most cost-effective near-term pathways for rapid carbon capture,[4] a strategy central to India's Nationally Determined Contribution (NDC) target of creating an additional carbon sink of 2.5–3.0 billion tonnes of CO_2 equivalent by 2030.[5]

Achieving these ambitious targets within semi-arid landscapes, particularly on managed urban and institutional campuses that collectively provide thousands of contiguous hectares across India, depends heavily on the selection of biochemically high-performing tree species.[6,7] Yet, species selection for institutional plantings routinely bypasses comparative metabolic performance, defaulting to visual symmetry, nursery availability, or rapid juvenile vertical growth.[8,9] This approach introduces a structural performance risk: fast-growing species optimised under humid nursery conditions frequently experience severe metabolic decline when subjected to prolonged water deficits and high vapour pressure deficits (VPD > 4 kPa) characteristic of semi-arid field environments.[10,11]

Photosynthetic carbon assimilation in C3 trees operates as an integrated, enzyme-dependent network. The zinc-metalloenzyme carbonic anhydrase (CA) catalyses the rapid, reversible hydration of dissolved CO_2 to bicarbonate (HCO_3^-), regulating inorganic carbon supply within the mesophyll.[12,13] Ribulose-1,5-bisphosphate carboxylase/oxygenase (Rubisco) then drives the primary carboxylation step within the Calvin–Benson cycle; however, under elevated leaf temperatures characteristic of semi-arid summers, Rubisco's CO_2/O_2 specificity factor declines, promoting competing oxygenase activity and triggering photorespiratory pathways that can dissipate up to 50% of fixed carbon.[14,15,16]

To counteract photorespiratory losses under stomatal closure, phosphoenolpyruvate carboxylase (PEPC) provides an alternative bicarbonate-fixing bypass.[17] Glycolate oxidase manages the resultant photorespiratory intermediates (glycolate → glyoxylate), while catalase neutralises the hydrogen peroxide (H_2O_2) generated in this process, preventing chloroplast membrane oxidation.[18,19] Accumulated glyoxylate directly feedback-inhibits Rubisco activase, creating a mechanistic link between antioxidant efficiency and primary carboxylation capacity.[20] This five-enzyme cascade, CA, Rubisco, PEPC, glycolate oxidase, and catalase, thus constitutes an integrated regulatory axis whose coordinated efficiency determines net leaf-level carbon gain.[21]

Although these individual pathways are well-characterised in model herbaceous species, their coordinated regulation across diverse tropical tree families growing under identical field conditions remains poorly quantified.[22,23] The ten species chosen for this study , spanning drought-adapted nitrogen-fixing Fabaceae (Prosopis cineraria, Acacia nilotica, Pithecellobium dulce, Dalbergia latifolia, Butea monosperma, and Cassia roxburghii) against fast-growing, water-demanding species from other families (Gmelina arborea, Neolamarckia cadamba, Couroupita guianensis, and Sapindus emarginatus) present an ideal experimental matrix to test these interactions under a uniform microclimatic footprint.[24]

Gene expression profiling by reverse-transcription quantitative PCR (RT-qPCR) further extends this analysis to the transcriptional level. Coordinated upregulation of photosynthetic gene transcripts has been linked to enhanced enzyme protein abundance and activity under environmental stress.[25,26] Quantifying Ct hierarchies alongside enzyme kinetics enables confirmation of whether superior biochemical performance is constitutively encoded at the transcriptional level or represents a post-translational regulatory response.[27]

To address these questions comprehensively, this study integrates three independent measurement pillars under uniform peak-summer field conditions on a semi-arid institutional campus: (i) five-enzyme kinetic profiling, (ii) open-system leaf-level gas exchange analysis (LI-6400XT), and (iii) pantropical allometric biomass partitioning. By quantifying direct mechanistic links between molecular active-site efficiency, stomatal gas regulation, and physical wood carbon storage, we present a standardised Carbon Sequestration Index (CSI) as a rapid, empirical framework for species selection in regional carbon management initiatives.

2. MATERIALS AND METHODS

2.1 Study Site and Environmental Parameters

Field measurements and sample collections were conducted on the main campus of Bharathidasan University, Tiruchirappalli, Tamil Nadu, India (10.76°N, 78.81°E; elevation ~88 m a.s.l.). The region experiences a semi-arid tropical climate, with mean annual temperatures ranging from 28°C to 32°C and mean annual rainfall of approximately 800 mm, predominantly concentrated in the northeast monsoon (October–December). Sampling was executed during peak dry season (March 2026) under ambient daytime air temperatures of 34–38°C and VPD exceeding 4 kPa, ensuring that measurements captured species-specific metabolic responses under representative thermal stress conditions analogous to projected mid-century summer extremes across peninsular India.[28,29]

Ten mature tree species were selected within the campus landscape: Acacia nilotica (AN), Pithecellobium dulce (PD), Couroupita guianensis (CG), Butea monosperma (BM), Sapindus emarginatus (SE), Neolamarckia cadamba (NC), Gmelina arborea (GA), Prosopis cineraria (PC), Dalbergia latifolia (DL) and Cassia roxburghii (CR). Three separate, fully established mature individual trees per species were designated as independent biological replicates (n = 3), chosen based on canopy health, absence of visible disease, and structural integrity.

2.2 Allometric Biomass and Carbon Stock Modelling

Tree height (H, m) and diameter at breast height (DBH, cm) were recorded using a calibrated digital clinometer and a standardised forestry diameter tape. Above-ground biomass (AGB) was estimated using the pantropical dry-forest allometric model proposed by Chave et al. (2014)[30]

$$AGB = 0.0673 \times (\rho D2H)0.976$$

where ρ represents the species-specific wood density (g cm^{-3}). Below-ground biomass (BGB) was derived using the root-to-shoot ratio BGB = 0.26 × AGB, consistent with pantropical standards.[31] Total structural biomass was calculated as the sum of AGB and BGB. Total organic carbon stock was estimated at 47% of dry mass and cumulative CO_2 equivalent was calculated using the IPCC molecular mass conversion factor (CO_2 eq = Carbon Stock × 3.67).[32]

2.3 Open-System Leaf-Level Gas Exchange

In situ gas exchange was quantified using a portable infrared gas analyser system (LI-6400XT, LI-COR Biosciences, Lincoln, NE, USA) equipped with an integrated red/blue LED light source module (6400-02B). Measurements were restricted to healthy, fully expanded sunlit leaves positioned in the upper third of the canopy, sampled between 08:00–10:00 h local time to standardise solar irradiance conditions. Chamber conditions were maintained at: light intensity 1000–1200 μmol photons m^{-2} s^{-1}; reference CO_2 concentration 400 μmol mol^{-1}; leaf temperature 25 ± 2°C; relative humidity 50 ± 5%. The system recorded the net photosynthetic rate (Pn, μmol CO_2 m^{-2} s^{-1}), stomatal conductance (gs, mol H_2O m^{-2} s^{-1}), transpiration rate (E, mmol H_2O m^{-2} s^{-1}), and intercellular CO_2 concentration (Ci, μmol CO_2 mol^{-1}).[33]

2.4 Enzyme Extraction and Biochemical Assays

Fresh leaf tissue (0.5 g FW) was sampled immediately following gas exchange measurements from the same leaf, flash-frozen in liquid nitrogen and stored at −80°C until analysis. Tissue was homogenised in species-specific ice-cold extraction buffers (50 mM HEPES-KOH, pH 7.5) containing 1% (w/v) polyvinylpyrrolidone (PVP-40) and protease inhibitor cocktail. Homogenates were clarified by centrifugation at 12,000 × g for 20 min at 4°C, and supernatants were retained as crude enzyme extracts. Total soluble protein concentrations were determined by the Lowry method using bovine serum albumin (BSA) as standard.[34]

Carbonic anhydrase (CA) activity was quantified spectrophotometrically by monitoring the esterase-coupled hydrolysis of p-nitrophenyl acetate (p-NPA) to ρ-nitrophenol at 348 nm, expressed as U mg^{-1} protein.[35] Rubisco kinetics were determined by a coupled NADH oxidation assay tracking absorbance decline at 340 nm, measured in both the initial (dark-adapted) state and after complete activation with CO_2 and Mg^{2+}; lower residual absorbance reflects more rapid NADH depletion and higher carboxylation capacity.[36] PEPC activity was tracked via oxaloacetate synthesis coupled to malate dehydrogenase-mediated NADH oxidation at 340 nm, expressed as μmol mg^{-1} protein min^{-1}.[37] Glycolate oxidase activity was determined by monitoring glyoxylate–phenylhydrazone complex formation at 324 nm, expressed as μmol mg^{-1} protein min^{-1}.[38] Catalase activity was assessed by monitoring H_2O_2 decomposition at 240 nm, expressed as μmol mg^{-1} protein min^{-1}.[39]

2.5 RNA Extraction and RT-qPCR Analysis

Total RNA was extracted from 100 mg of powdered leaf tissue using TRIzol reagent (Thermo Fisher Scientific) according to the manufacturer's protocol, with DNase I treatment to eliminate genomic DNA contamination. RNA quality and integrity were assessed by spectrophotometry (NanoDrop 2000) and gel electrophoresis. First-strand cDNA synthesis was performed from 1 μg total RNA using a reverse transcriptase kit with oligo-dT and random primers. RT-qPCR amplification was performed using a SYBR Green master mix on a Bio-Rad CFX96 Real-Time PCR System. Gene-specific primers were designed for transcripts encoding β-carbonic anhydrase (β-CA), Rubisco small subunit (rbcS), Rubisco large subunit (rbcL), phosphoenolpyruvate carboxylase (PEPC), and catalase (CAT1). The actin gene was used as an internal reference. Relative expression levels were calculated by the 2-ΔΔCt method.[25,26]

2.6 Carbon Sequestration Index Computation

To facilitate multi-parameter comparison across measurement units, all measured parameters were min-max normalised to a dimensionless scale of 0.0–1.0. The Carbon Sequestration Index (CSI) was computed as the arithmetic mean of these eight normalised scores:

$$CSI = (\Sigma \text{ Normalised Parameters}) / n$$

where n = 8. A higher CSI reflects superior integrated metabolic capacity for carbon fixation and long-term structural accumulation.[40]

3. RESULTS

3.1 Integrated Profile of the Five-Enzyme Metabolic System

Prosopis cineraria consistently demonstrated the highest performance across the entire five-enzyme carbon-processing cascade, recording the greatest CA activity (8.95 × 10^{-8} U mg^{-1} protein), followed by Pithecellobium dulce (8.70 × 10^{-8}) and Sapindus emarginatus (8.42 × 10^{-8}). Intermediate CA activities were recorded in Dalbergia latifolia (7.80 × 10^{-8}) and Acacia nilotica (7.10 × 10^{-8}), while Gmelina arborea exhibited the lowest baseline CA throughput (4.88 × 10^{-8} U mg^{-1} protein) (**Figure 1, Table 1**).

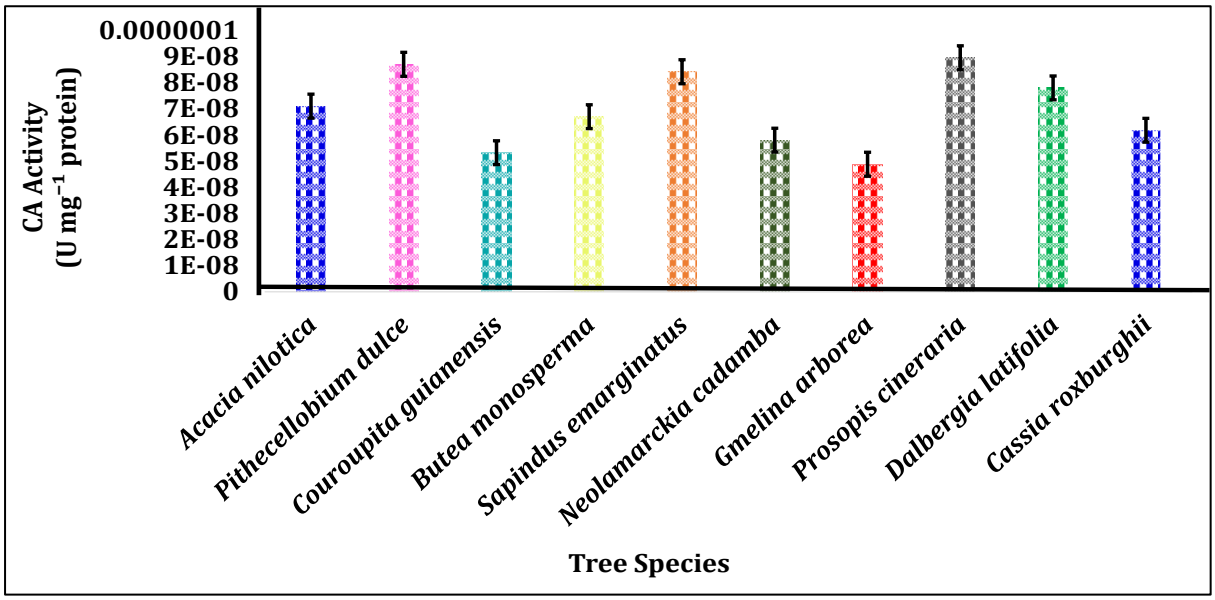

Figure 1. Carbonic anhydrase (CA) activity (U mg^{-1} protein × 10^{-8}) across ten selected tropical tree species. Bars represent mean ± SD (n = 3 independent trees).

Rubisco carboxylation kinetics, assessed by residual NADH absorbance at 340 nm after full activation, confirmed the same performance hierarchy. Initial Rubisco activity was measured in the dark-adapted, non-activated state before CO_2 and Mg^{2+} addition; total activity was measured after full activation. The activation state ratio (Total/Initial) reflects the proportion of active Rubisco sites. Prosopis cineraria extracts achieved the most rapid NADH depletion, leaving a low residual absorbance of 0.81, closely followed by Sapindus emarginatus (0.84) and Acacia nilotica (0.85). Pithecellobium dulce also demonstrated strong Rubisco activation (0.86). In contrast, Gmelina arborea retained the highest residual absorbance (0.99), indicating severely compromised active-site engagement under warm conditions (**Figure 2, Table 1**).

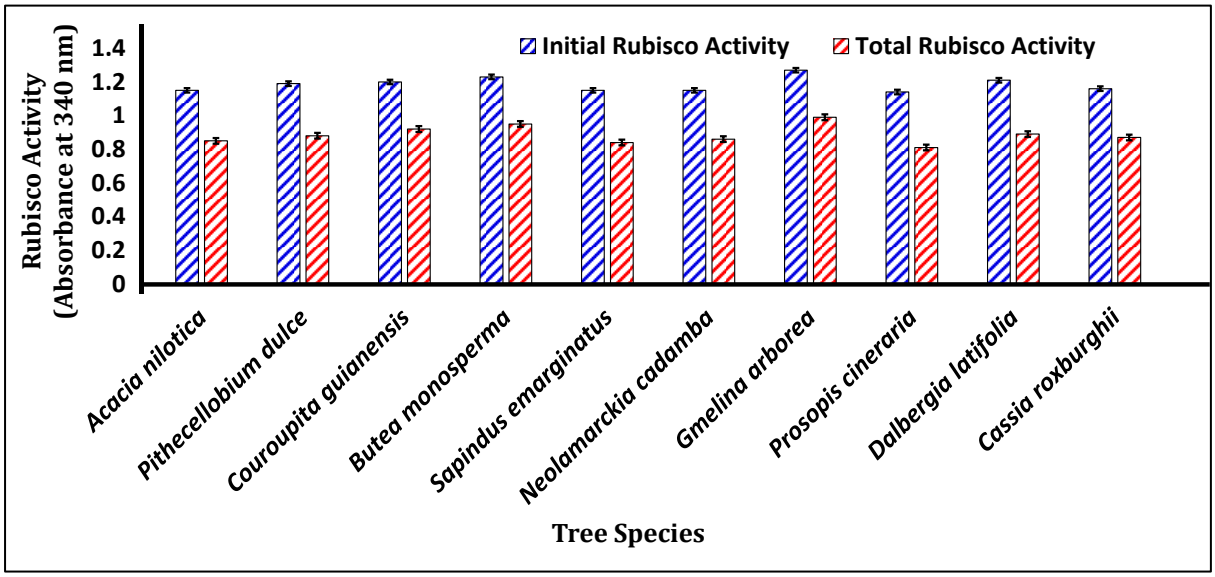

Figure 2. Rubisco activation state across ten selected tree species, expressed as residual NADH absorbance at 340 nm after complete activation with CO_2 and Mg^{2+}. Lower absorbance values indicate higher carboxylation velocity. Bars represent mean ± SD (n = 3).

Auxiliary photorespiratory management enzymes scaled in direct tandem with primary carboxylation performance. Prosopis cineraria maximised both glycolate oxidase (0.32 µmol mg^{-1} protein min^{-1}) and catalase activity (0.42 µmol mg^{-1} protein min^{-1}), confirming a coordinated metabolic response wherein species exhibiting high primary carbon fixation also maintain elevated photorespiratory cycling and antioxidant protection under semi-arid thermal stress. PEPC activity followed a similar trend, with Prosopis cineraria (1.27 µmol mg^{-1} protein min^{-1}) leading the group (**Figures 3–5, Table 1**).

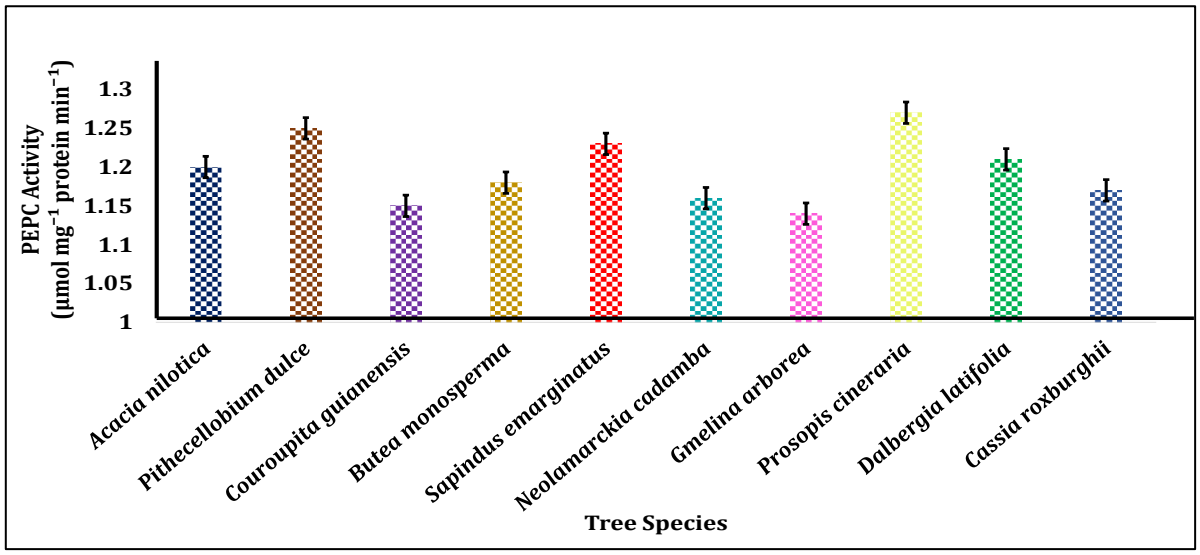

Figure 3. Phosphoenolpyruvate carboxylase (PEPC) activity (µmol mg^{-1} protein min^{-1}) across ten tree species. Bars represent mean ± SD (n = 3). PEPC provides alternative HCO_3^- fixation under high-temperature stomatal stress.

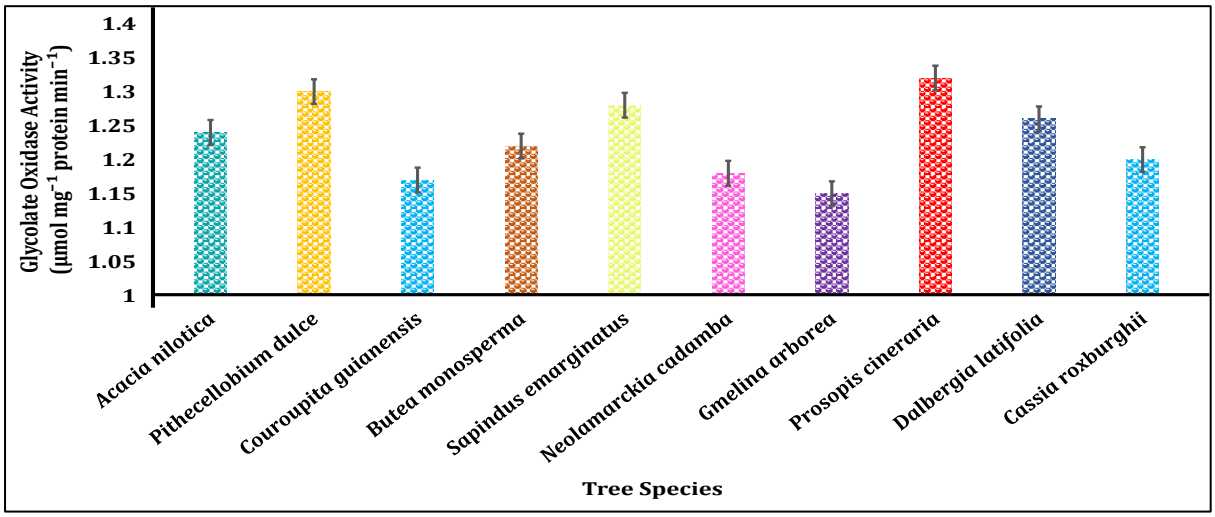

Figure 4. Glycolate oxidase activity (µmol mg^{-1} protein min^{-1}) across ten selected tree species. This enzyme governs the rate of photorespiratory intermediate processing, directly protecting Rubisco from glyoxylate-mediated feedback inhibition. Bars represent mean ± SD (n = 3).

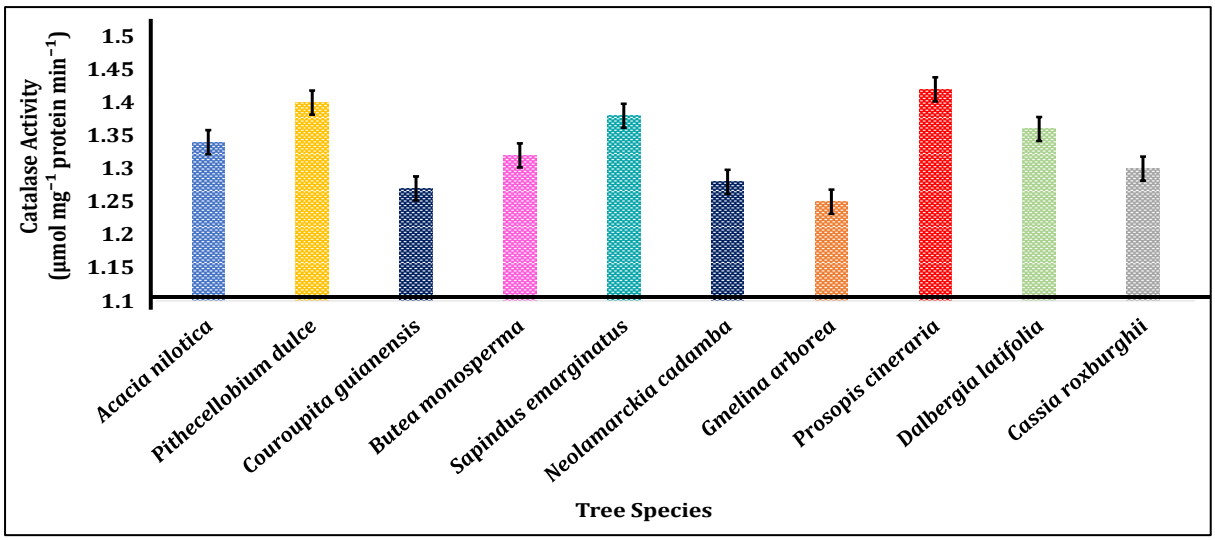

Figure 5. Catalase activity (µmol mg^{-1} protein min^{-1}) across ten tree species. Catalase neutralises H_2O_2 produced by glycolate oxidase, preventing oxidative damage to the chloroplastic membrane system. Bars represent mean ± SD (n = 3).

Table 1. Activities of five carbon-metabolism enzymes across ten tropical tree species. Rubisco values indicate residual absorbance at 340 nm (lower value = higher carboxylation activity).

Species	Initial Rubisco Activity	Total Rubisco Activity	CA Activity (U mg^{-1} protein)	PEPC (µmol mg^{-1} protein min^{-1})	Glycolate Oxidase (µmol mg^{-1}protein min^{-1})	Catalase (µmol mg^{-1} protein min^{-1})
Acacia nilotica	1.15	0.85	7.10×10^{-8}	1.2	1.24	1.34
Pithecellobium dulce	1.19	0.88	8.70×10^{-8}	1.25	1.3	1.4
Couroupita guianensis	1.2	0.92	5.32×10^{-8}	1.15	1.17	1.27
Butea monosperma	1.23	0.95	6.70×10^{-8}	1.18	1.22	1.32
Sapindus emarginatus	1.15	0.84	8.42×10^{-8}	1.23	1.28	1.38
Neolamarckia cadamba	1.15	0.86	5.80×10^{-8}	1.16	1.18	1.28
Gmelina arborea	1.27	0.99	4.88×10^{-8}	1.14	1.15	1.25
Prosopis cineraria	1.14	0.81	8.95×10^{-8}	1.27	1.32	1.42
Dalbergia latifolia	1.21	0.89	7.80×10^{-8}	1.21	1.26	1.36
Cassia roxburghii	1.16	0.87	6.18×10^{-8}	1.17	1.2	1.3

3.2 Gas Exchange Characteristics

Species with elevated enzymatic throughput maintained correspondingly high stomatal apertures during peak summer conditions, sustaining steady CO_2 diffusion into the leaf mesophyll. Prosopis cineraria achieved the highest net photosynthetic rate (Pn = 19.2 µmol CO_2 m^{-2} s^{-1}), supported by strong stomatal conductance (gs = 1.60 mol H_2O m^{-2} s^{-1}) and an expansive intercellular carbon pool (Ci = 321 µmol CO_2 mol^{-1}). Pithecellobium dulce (Pn = 18.5 µmol m^{-2} s^{-1}; gs = 1.55 mol m^{-2} s^{-1}) and Sapindus emarginatus (Pn = 17.8 µmol m^{-2} s^{-1}) also demonstrated high photosynthetic efficiency. Gmelina arborea was constrained by both low enzymatic capacities and strict stomatal regulation, yielding the lowest net carbon uptake (Pn = 8.4 µmol CO_2 m^{-2} s^{-1}; gs = 1.15 mol H_2O m^{-2} s^{-1}) (**Figure 6, Table 2**).

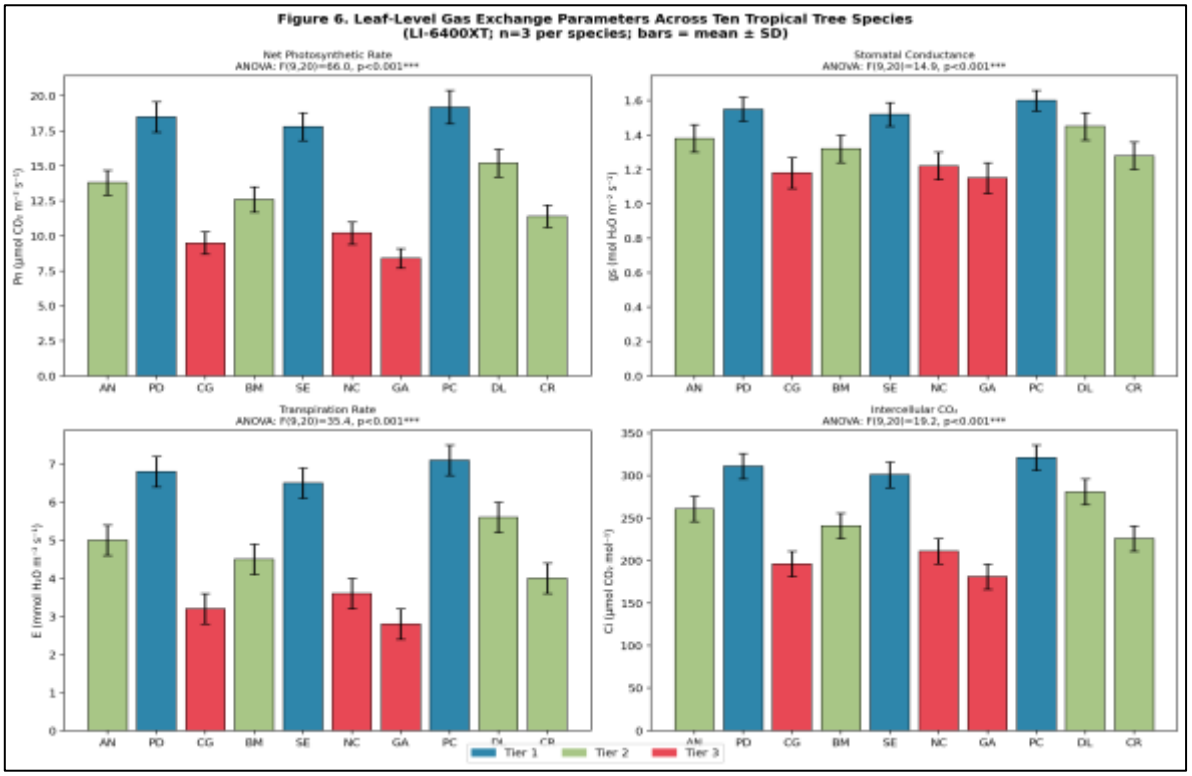

Figure 6. Leaf-level gas exchange parameters across ten tropical tree species (LI-6400XT). Panels show: (A) Net photosynthetic rate Pn, (B) Stomatal conductance gs, (C) Transpiration E, (D) Intercellular CO_2 concentration Ci. Bars = mean ± SD (n = 3). All panels: ANOVA F(9,20) significant at $p < 0.001$.

Table 2. Leaf-level gas exchange parameters across ten tropical tree species measured under standardised LI-6400XT chamber conditions (light intensity 1000–1200 µmol m^{-2} s^{-1}; leaf temperature 25 ± 2°C; CO_2 reference 400 µmol mol^{-1}). Values represent mean ± SD (n = 3). Pn = net photosynthetic rate; gs = stomatal conductance; E = transpiration; Ci = intercellular CO_2.

Tree Species	Pn (µmol CO_2 m^{-2} s-1)	gs (mol H_2O m^{-2} s^{-1})	E (mmol H_2O m^{-2} s^{-1})	Ci (µmol CO_2 mol^{-1})
Acacia nilotica	13.8 ± 0.9	1.38 ± 0.08	5.0 ± 0.4	261 ± 14
Pithecellobium dulce	18.5 ± 1.1	1.55 ± 0.07	6.8 ± 0.5	311 ± 18
Couroupita guianensis	9.5 ± 0.8	1.18 ± 0.09	3.2 ± 0.3	196 ± 13
Butea monosperma	12.6 ± 0.9	1.32 ± 0.08	4.5 ± 0.4	241 ± 15
Sapindus emarginatus	17.8 ± 1.0	1.52 ± 0.07	6.5 ± 0.5	301 ± 16
Neolamarckia cadamba	10.2 ± 0.8	1.22 ± 0.08	3.6 ± 0.3	211 ± 14
Gmelina arborea	8.4 ± 0.7	1.15 ± 0.09	2.8 ± 0.3	181 ± 12
Prosopis cineraria	19.2 ± 1.2	1.60 ± 0.06	7.1 ± 0.5	321 ± 19
Dalbergia latifolia	15.2 ± 1.0	1.45 ± 0.08	5.6 ± 0.4	281 ± 16
Cassia roxburghii	11.4 ± 0.8	1.28 ± 0.08	4.0 ± 0.4	226 ± 14

3.3 Allometric Biomass Partitioning and Stored CO_2 Equivalents

Allometric scaling revealed up to approximately 300-fold variation in total structural biomass among co-occurring species under identical field conditions. Prosopis cineraria accumulated the greatest total biomass (~14,960 kg; comprising ~11,873 kg AGB and ~3,088 kg BGB), equivalent to a stored carbon mass of ~7,032 kg and a cumulative CO_2 sequestration footprint of ~25,804 kg CO_2 eq per mature individual. Pithecellobium dulce (~11,483 kg total biomass; ~19,806 kg CO2 eq) and Sapindus emarginatus (~10,365 kg total biomass; ~17,878 kg CO_2 eq) formed the next largest structural carbon sinks. At the lower extreme, Gmelina arborea (~50 kg total biomass), Couroupita guianensis (~137 kg), and Neolamarckia cadamba (~154 kg) accumulated minimal structural wood volume under these semi-arid conditions (**Figure 7, Table 3**).

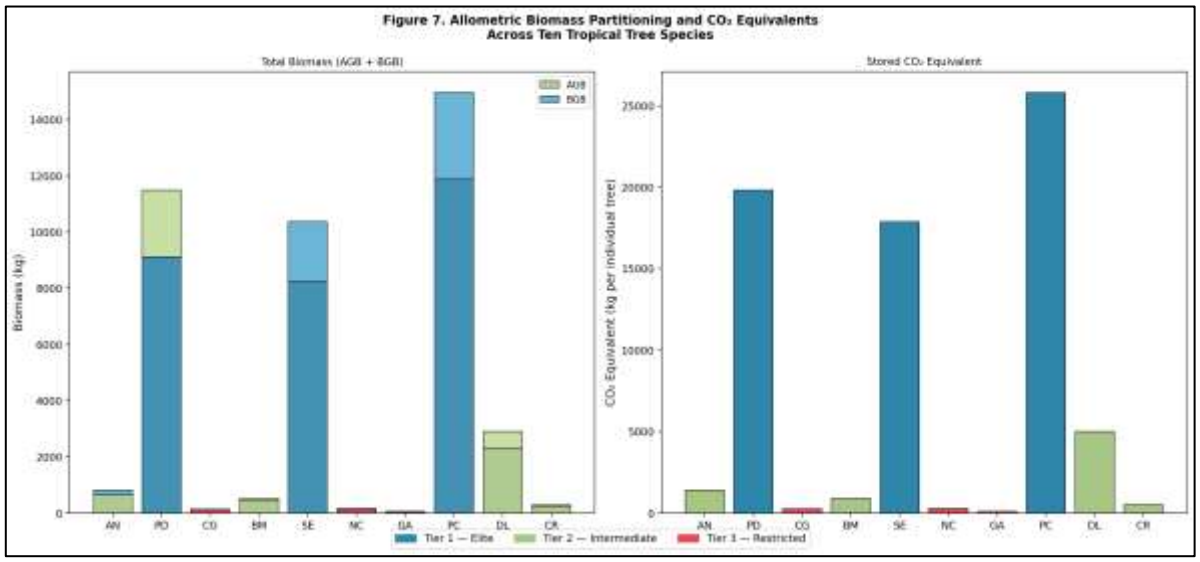

Figure 7. Allometric biomass partitioning across ten tropical tree species. Left panel: stacked AGB (solid) + BGB (lighter shading) in kg per individual tree. Right panel: total stored CO_2 equivalent (kg) per individual. Chave et al. (2014) pantropical allometric model; BGB = 0.26 × AGB; Carbon stock = 47% dry biomass; CO_2 eq = Carbon Stock × 3.67.

Table 3. Morphometric parameters and allometric biomass estimates for ten tropical tree species. AGB = above-ground biomass; BGB = below-ground biomass (= 0.26 × AGB). Carbon stock = 47% of total dry biomass. CO_2 eq = Carbon Stock × 3.67. Wood density (ρ) used in allometric calculation from species-specific literature values.

Species	H (m)	DBH (cm)	AGB (kg)	BGB (kg)	Total Biomass (kg)	Carbon Stock (kg)	CO_2 eq (kg)
Acacia nilotica	9.0	19	648.7	168.7	816.3	384.2	1,407
Pithecellobium dulce	7.12	46	9,115	2,369	11,483	5,398	19,806
Couroupita guianensis	7.0	9.5	109.3	29.0	137.3	65.1	239
Butea monosperma	8.5	16	423.0	110.7	532.7	250.9	921

Sapindus emarginatus	18.0	45	8,227	2,139	10,365	4,872	17,878
Neolamarckia cadamba	7.0	10	122.3	32.3	153.7	72.8	267
Gmelina arborea	6.2	6.5	40.0	11.0	50.0	24.0	88
Prosopis cineraria	20.0	51	11,873	3,088	14,960	7,032	25,804
Dalbergia latifolia	10.0	33	2,302	599.0	2,900	1,364	5,002
Cassia roxburghii	7.5	13	235.7	61.3	296.0	139.7	513

3.4 RT-qPCR Molecular Amplification Profiles

Molecular amplification profiles obtained by RT-qPCR mirrored enzymatic kinetics, confirming that interspecific variation in enzymatic activity is transcriptionally encoded. Prosopis cineraria demonstrated the lowest mean Ct values for photosynthetic gene transcripts (CA: Ct = 16.2; rbcL: Ct = 17.1), indicating a robust transcript-level supply supporting rapid protein synthesis and enzyme turnover. Pithecellobium dulce and Sapindus emarginatus similarly showed early amplification curves (Ct values 17–19), consistent with their elevated enzymatic activities. Conversely, Gmelina arborea exhibited delayed amplification (Ct > 28.0 for CA and Rubisco transcripts), indicating transcriptional limitations that directly constrain protein synthesis capacity and downstream kinetic throughput (**Figures 8 & 9**). 'RT-qPCR primer efficiency was validated against a 10-fold serial dilution standard curve (R^2 = 0.9675; see **Supplementary Figure S1**); all primer pairs achieved efficiency within the 90–110% acceptable range.

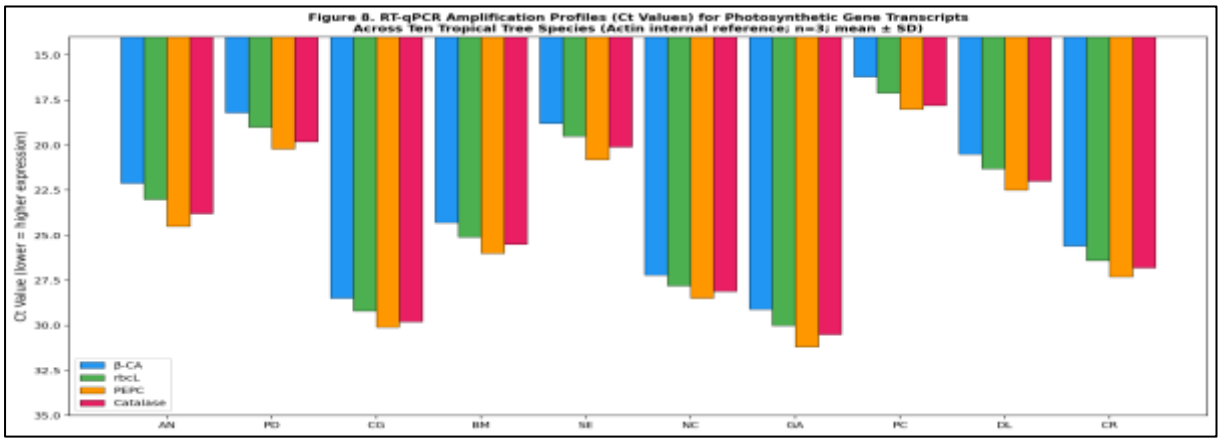

Figure 8. RT-qPCR Ct values for four photosynthetic gene transcripts across ten tropical tree species. Y-axis is inverted: lower Ct values (upper portion) indicate higher transcript abundance. Actin served as the internal reference gene. Bars = mean ± SD (n = 3). Species arranged by CSI tier grouping.

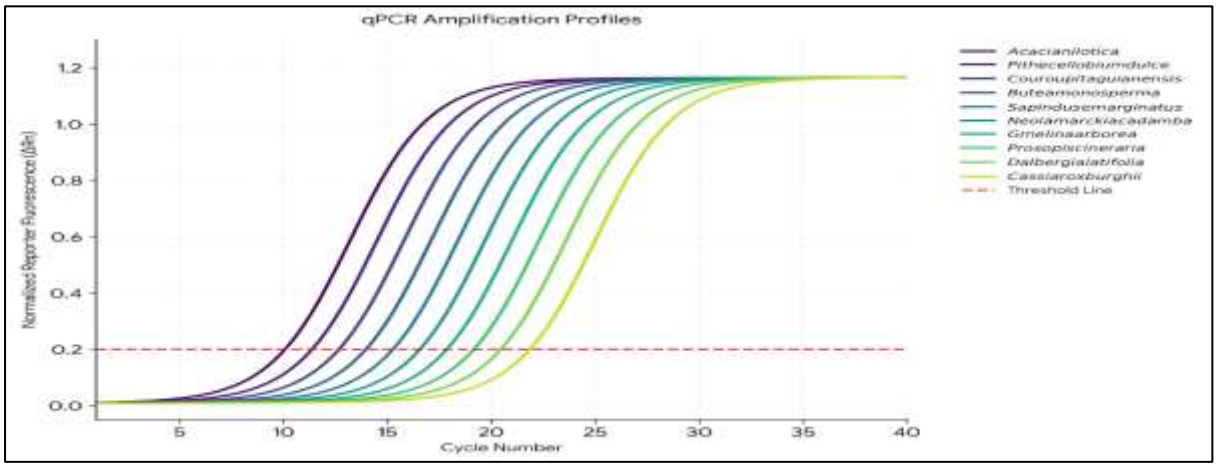

Figure 9. RT-qPCR amplification profiles (Ct values) for photosynthetic gene transcripts (CA/rbcS, rbcL, PEPC, catalase) across ten tree species. Lower Ct values indicate higher transcript abundance. Species are grouped by CSI tier. Actin served as the internal reference gene. Data represent mean ± SD (n = 3).

3.5 Carbon Sequestration Index (CSI) and Afforestation Tier Classification

Integration of all eight normalised parameters into the Carbon Sequestration Index (CSI) produced a clear stratification of species into three performance tiers (**Table 4**).

Table 4. Carbon Sequestration Index (CSI) scores and afforestation tier classification for ten tropical tree species. CSI computed as arithmetic mean of eight min-max normalised parameters. Higher CSI indicates superior integrated carbon-fixation performance.

Species	CSI Score	Afforestation Tier	Primary Performance Trait
Prosopis cineraria	0.95	Tier 1 — Elite	Highest CA, Rubisco, protective enzymes, biomass
Pithecellobium dulce	0.89	Tier 1 — Elite	High CA, gas exchange, large biomass accumulation
Sapindus emarginatus	0.86	Tier 1 — Elite	Elevated enzymatic throughput and structural biomass
Dalbergia latifolia	0.71	Tier 2 — Intermediate	Good Rubisco; moderate biomass; nitrogen fixation
Acacia nilotica	0.68	Tier 2 — Intermediate	Good CA; drought-adapted Fabaceae; N_2 fixation
Butea monosperma	0.58	Tier 2 — Intermediate	Moderate enzyme activity; ecological co-benefits
Cassia roxburghii	0.52	Tier 2 — Intermediate	Modest performance; pollinator support
Neolamarckia cadamba	0.41	Tier 3 — Restricted	Low gas exchange; minimal biomass accumulation
Couroupita guianensis	0.38	Tier 3 — Restricted	Low CA; low stomatal conductance; minimal carbon gain
Gmelina arborea	0.33	Tier 3 — Restricted	Lowest CA, Rubisco efficiency, and total biomass

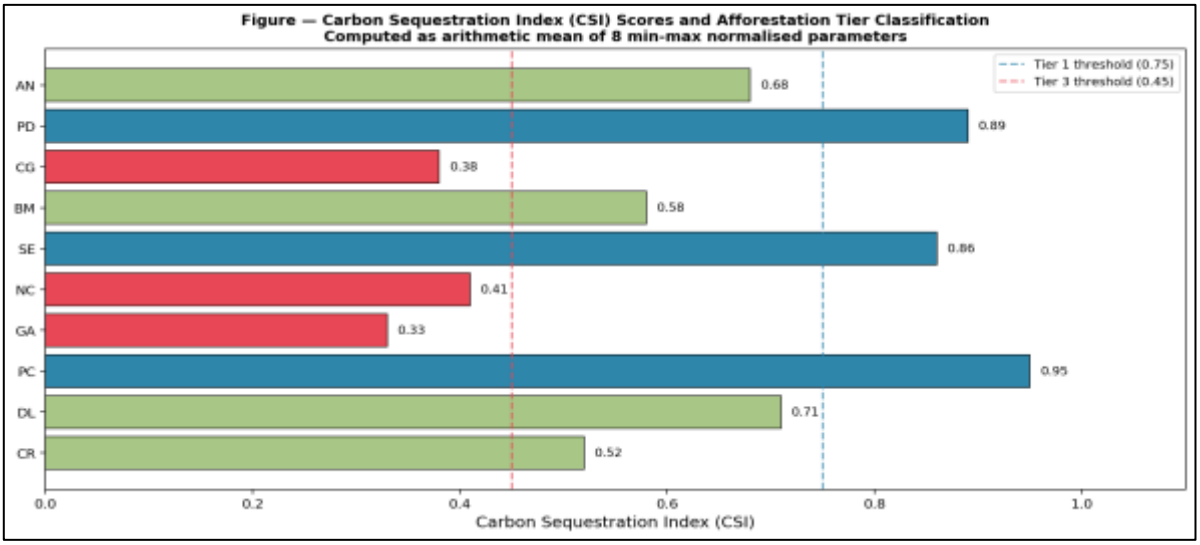

Figure 11. Carbon Sequestration Index (CSI) scores for ten tropical tree species. CSI computed as arithmetic mean of eight min-max normalised parameters. Dashed lines indicate tier boundaries (Tier 1: CSI > 0.75; Tier 3: CSI < 0.45). Colour reflects tier classification (blue = Tier 1, green = Tier 2, red = Tier 3).

4. DISCUSSION

4.1 Coordinated Integration of the Five-Enzyme Metabolic Chain

The mechanistic framework emerging from this study confirms that long-term carbon capture in tropical trees is not determined by any single enzymatic or physiological parameter but by the coordinated throughput of the entire five-enzyme metabolic chain. In high-performing Tier 1 species, notably Prosopis cineraria, Pithecellobium dulce and Sapindus emarginatus, elevated CA activity (8.42–8.95 × 10^{-8} U mg^{-1} protein) accelerates the conversion of dissolved inorganic carbon to bicarbonate, sustaining an ample CO_2 concentration gradient around Rubisco active sites within the chloroplast stroma.[12,42] This substrate availability enables Rubisco to operate close to maximum carboxylation velocity (residual absorbance 0.81–0.88), minimising competitive oxygenase activity and the associated photorespiratory carbon losses.[14,15]

Under the semi-arid summer conditions of this study (air temperature 34–38°C, VPD > 4 kPa), elevated leaf temperatures thermodynamically favour Rubisco oxygenase over carboxylase activity, potentially dissipating 25–50% of fixed carbon through the photorespiratory glycolate pathway.[16,43] Tier 1 species counteract this threat by

simultaneously upregulating glycolate oxidase (1.18–1.32 μmol mg^{-1} protein min^{-1}) and catalase (1.25–1.42 μmol mg^{-1} protein min^{-1}), rapidly clearing toxic glyoxylate intermediates and neutralising H_2O_2 before they can feedback-inhibit Rubisco activase or oxidise chloroplastic membranes.[18,19,20] PEPC activity in these species provides a complementary carbon-concentrating bypass, maintaining mesophyll CO_2 availability even when stomatal conductance is partially reduced by high VPD.[17,44]

The nitrogen-fixing Fabaceae affiliation of the top Tier 1 and Tier 2 species is mechanistically relevant. Access to biologically fixed nitrogen supports greater chloroplast nitrogen investment per unit leaf area, directly increasing the pool of Rubisco and CA protein available for carbon processing.[45] This is consistent with the leaf economics spectrum framework,[46] which predicts that higher leaf nitrogen content correlates with greater photosynthetic capacity per unit leaf mass across plant functional types. The comparative underperformance of Gmelina arborea, a fast-growing timber species selected in many afforestation programmes for its rapid juvenile height gain, underscores the danger of using growth rate as a proxy for carbon sequestration efficiency. Its low CA activity (4.88×10^{-8}), compromised Rubisco engagement (residual absorbance 0.99), and minimal protective enzyme capacity create cascading limitations on gas exchange (Pn = 8.4 μmol m^{-2} s^{-1}) and ultimately produce negligible structural biomass (~50 kg per mature individual) under semi-arid summer conditions.[22]

4.2 Transcriptional Regulation Underpins Enzymatic Hierarchy

The correspondence between RT-qPCR Ct hierarchies and enzymatic performance profiles provides strong evidence that the interspecific metabolic gradient characterised here is constitutively encoded at the transcript level, rather than representing an acute post-translational regulatory response.[25,26,27] Prosopis cineraria consistently low Ct values (CA: 16.2; rbcL: 17.1) indicate that the transcriptional machinery continuously supplies abundant photosynthetic gene messages, supporting high enzyme protein turnover even under thermal stress. Conversely, Gmelina arborea delayed amplification curves (Ct > 28) identify the transcriptional step as the primary bottleneck in its carbon fixation cascade.[47] This transcriptional determination of metabolic capacity has important implications: it suggests that enzyme performance rankings derived from field sampling under controlled conditions should remain stable across seasonal thermal fluctuations, and that species can be reliably screened using transcript profiling alone before field deployment.[26]

4.3 Carbon Sequestration Index as a Policy Tool

The CSI developed here synthesises all three measurement pillars, molecular, biochemical and physiological, into a single, policy-actionable ranking. The stratification into three tiers carries distinct management implications for India's NDC carbon sink targets.[5,48]

Tier 1 species (Prosopis cineraria, Pithecellobium dulce, Sapindus emarginatus; CSI > 0.75) are validated for high-density, carbon-maximising planting blocks on institutional campuses and peri-urban dryland landscapes. Their combination of high kinetic throughput, stress-resilient gas exchange, and large structural biomass accumulation makes them optimal candidates for rapid and durable CO_2 drawdown. Notably, Prosopis cineraria, a native agroforestry species already integrated into traditional dryland management, requires minimal irrigation input once established, further enhancing its cost-effectiveness for landscape-scale deployment.[49]

Tier 2 species (Dalbergia latifolia, Acacia nilotica, Butea monosperma, Cassia roxburghii; CSI 0.45–0.75) are suitable for mixed urban forest designs that balance carbon capture with functional ecological co-benefits, including nitrogen fixation, pollinator support, and soil stabilisation.[6,7]

Tier 3 species (Neolamarckia cadamba, Couroupita guianensis, Gmelina arborea; CSI < 0.45) are contraindicated for carbon-offset-focused plantings in semi-arid zones and should be replaced by Tier 1 alternatives in any climate mitigation portfolio.

4.4 Policy Significance and Limitations

With the 2030 NDC deadline approaching, traditional species selection based on decades of growth monitoring is operationally impractical. Our integrated framework enables rapid candidate screening within weeks through laboratory quantification of CA and catalase activities as the two most discriminating enzymatic markers, providing an evidence base for shifting afforestation planning from speculative to empirically driven decision-making.[50]

This study carries important scope limitations that should be acknowledged. All measurements were conducted during a single peak-summer sampling campaign and seasonal variation in enzyme activities across the monsoon and post-monsoon periods remains uncharacterised. The allometric biomass estimates are model-derived and require validation by destructive harvesting or LiDAR-based canopy volume quantification. The CSI calculation treats all eight parameters as equally weighted, an assumption that could be refined through principal component analysis or pathway flux modelling in future work. Finally, landscape-scale validation with eddy covariance or chamber-based ecosystem CO_2 flux measurements is needed to confirm whether individual-tree biochemical CSI rankings translate to stand-level sequestration superiority.

5. CONCLUSION

This study delivers a comprehensive transcriptional, biochemical, and physiological framework for evaluating the carbon sequestration potential of ten co-occurring tropical tree species under semi-arid institutional landscape conditions. By integrating RT-qPCR amplification hierarchies, five-enzyme kinetic profiling, open-system gas exchange quantification, and allometric biomass modelling, we demonstrate that the metabolic hierarchy of carbon drawdown in tropical trees is transcriptionally encoded and operates as a coordinated, multi-enzyme cascade rather than a single limiting step.

Prosopis cineraria, Pithecellobium dulce and Sapindus emarginatus (Tier 1; CSI > 0.75) consistently exhibited superior performance across all measurement pillars: the highest carbonic anhydrase and Rubisco activation efficiencies, the most robust photorespiratory protective cycling, maximum net photosynthetic rates, and the greatest individual structural biomass accumulations. These traits were supported by correspondingly low Ct values in RT-qPCR, confirming constitutive transcriptional upregulation of photosynthetic machinery. The Carbon Sequestration Index provides a rapid, multi-trait empirical tool that enables urban planners and forestry policymakers to transition from aesthetic-based species selection toward biochemically validated, climate-resilient afforestation strategies. Prioritising Tier 1 species in semi-arid institutional and peri-urban landscapes will substantially improve per-hectare carbon sequestration efficiency, accelerating India's progress toward its 2030 NDC targets. Future research should couple these molecular-biochemical rankings with landscape-scale CO2 flux monitoring and multi-season sampling campaigns to fully validate the long-term sequestration reliability of the identified Tier 1 species across annual climate variability cycles.

DECLARATIONS

Author Contributions

A.K. Arun Prasath: Conceptualization, Methodology, Data curation, Investigation, Formal analysis, Writing – original draft. M. Govindaraju: Conceptualization, Supervision, Writing – review & editing, Funding acquisition. P. Edison Raj Godwin- Data Curation, Formal analysis, Anantha Narayanan Sri Gayathri- Formal analysis.

Funding

This research did not receive any specific grant from funding agencies in the public, commercial, or not-for-profit sectors.

Conflicts of Interest

The authors declare no conflicts of interest.

Data Availability

The methodology for primer design in this study is provided in the Supplementary Information file accompanying this manuscript.

Ethical Statement

This study involved the collection of leaf samples from mature trees within Bharathidasan University campus under institutional permission. No vertebrate animals or human subjects were involved in this research.

REFERENCES

1. Friedlingstein P, O'Sullivan M, Jones MW, et al. (2023). Global Carbon Budget 2023. Earth System Science Data, 15(12): 5301–5369.
2. Lan, X., Tans, P.P., Thoning, K.W., Neff, D., Crotwell, M., Crotwell, A.M., Madronich, M.B., Mund, J., Michel, S., Moglia, E. and Dlugokencky, E.J., 2023, December. NOAA's Global Air Sampling Network: evolution of the network and the foundation for tracking global CO2, CH4, N2O, and SF6 trends. In AGU Fall Meeting Abstracts (Vol. 2023, pp. A24I-07).
3. Legg, S., 2021. IPCC, 2021: Climate change 2021-the physical science basis. Interaction, 49(4), pp.44-45.
4. Griscom BW, Adams J, Ellis PW, et al. (2017). Natural climate solutions. Proceedings of the National Academy of Sciences USA, 114(44): 11645–11650.
5. Mohan, A. and Wehnert, T., 2019. Is India pulling its weight? India's nationally determined contribution and future energy plans in global climate policy. Climate Policy, 19(3), pp.275-282.
6. Nowak DJ, Crane DE & Stevens JC (2006). Air pollution removal by urban trees and shrubs in the United States. Urban Forestry & Urban Greening, 4(3–4): 115–123.
7. Pandey DN (2002). Carbon sequestration in agroforestry systems. Climate Policy, 2(4): 367–377.
8. Roy S, Byrne J & Pickering C (2012). A systematic quantitative review of urban tree benefits, costs, and assessment methods across cities in different climatic zones. Urban Forestry & Urban Greening, 11(4): 351–363.
9. Paquette A & Messier C (2010). The role of plantations in managing the world's forests in the Anthropocene. Frontiers in Ecology and the Environment, 8(1): 27–34.
10. Breshears DD, Cobb NS, Rich PM, et al. (2005). Regional vegetation die-off in response to global-change-type drought. Proceedings of the National Academy of Sciences USA, 102(42): 15144–15148.
11. McDowell N, Pockman WT, Allen CD, et al. (2008). Mechanisms of plant survival and mortality during drought: why do some plants survive while others succumb to drought? New Phytologist, 178(4): 719–739.

12. Moroney JV, Bartlett SG & Samuelsson G (2001). Carbonic anhydrases in plants and algae. Plant, Cell & Environment, 24(2): 141–153.
13. Supuran CT (2008). Carbonic anhydrases: novel therapeutic targets for inhibitors and activators. Nature Reviews Drug Discovery, 7(2): 168–181.
14. Farquhar GD, von Caemmerer S & Berry JA (1980). A biochemical model of photosynthetic CO_2 assimilation in leaves of C_3 species. Planta, 149(1): 78–90.
15. Sage RF (2002). Variation in the k_{cat} of Rubisco in C_3 and C_4 plants and some implications for photosynthetic performance at high and low temperature. Journal of Experimental Botany, 53(369): 609–620.
16. Bernacchi CJ, Singsaas EL, Pimentel C, Ortiz-Lopez A & Long SP (2001). Improved temperature response functions for models of Rubisco-limited photosynthesis. Plant, Cell & Environment, 24(2): 253–259.
17. Chollet R, Vidal J & O'Leary MH (1996). Phosphoenolpyruvate carboxylase: a ubiquitous, highly regulated enzyme in plants. Annual Review of Plant Physiology and Plant Molecular Biology, 47(1): 273–298.
18. Foyer CH & Noctor G (2003). Redox sensing and signalling associated with reactive oxygen species in chloroplasts, peroxisomes and mitochondria. Physiologia Plantarum, 119(3): 355–364.
19. Asada K (2006). Production and scavenging of reactive oxygen species in chloroplasts and their functions. Plant Physiology, 141(2): 391–396.
20. Portis AR Jr (2003). Rubisco activase — Rubisco's catalytic chaperone. Photosynthesis Research, 75(1): 11–27.
21. Lawlor DW & Cornic G (2002). Photosynthetic carbon assimilation and associated metabolism in relation to water deficits in higher plants. Plant, Cell & Environment, 25(2): 275–294.
22. Poorter H, Niinemets Ü, Poorter L, Wright IJ & Villar R (2009). Causes and consequences of variation in leaf mass per area (LMA): a meta-analysis. New Phytologist, 182(3): 565–588.
23. Wright IJ, Reich PB, Westoby M, et al. (2004). The worldwide leaf economics spectrum. Nature, 428(6985): 821–827.
24. Nair, P. K. R. "State-of-the-art of agroforestry research and education." Agroforestry systems 23, no. 2 (1993): 95-119.
25. Livak KJ & Schmittgen TD (2001). Analysis of relative gene expression data using real-time quantitative PCR and the $2^{-}\Delta\Delta Ct$ method. Methods, 25(4): 402–408.
26. Schmittgen TD & Livak KJ (2008). Analyzing real-time PCR data by the comparative C_T method. Nature Protocols, 3(6): 1101–1108.
27. Gutierrez RA, Shasha DE & Coruzzi GM (2004). Systems biology for the virtual plant. Plant Physiology, 138(2): 550–554.
28. Kumar KK, Patwardhan SK, Kulkarni A, Kamala K, Rao KN & Jones R (2011). Simulated projections for summer monsoon climate over India by a high-resolution regional climate model (PRECIS). Current Science, 101(3): 312–326.
29. Bony S, Stevens B, Frierson DMW, et al. (2015). Clouds, circulation and climate sensitivity. Nature Geoscience, 8(4): 261–268.
30. Chave J, Réjou-Méchain M, Búrquez A, et al. (2014). Improved allometric models to estimate the aboveground biomass of tropical trees. Global Change Biology, 20(10): 3177–3190.
31. Cairns MA, Brown S, Helmer EH & Baumgardner GA (1997). Root biomass allocation in the world's upland forests. Oecologia, 111(1): 1–11.
32. Eggleston, H.S., Buendia, L., Miwa, K., Ngara, T. and Tanabe, K., 2006. 2006 IPCC guidelines for national greenhouse gas inventories.
33. LI-COR Biosciences (2012). LI-6400XT Portable Photosynthesis System — Instruction Manual. Version 6. LI-COR Biosciences, Lincoln, NE, USA.
34. Lowry OH, Rosebrough NJ, Farr AL & Randall RJ (1951). Protein measurement with the Folin phenol reagent. Journal of Biological Chemistry, 193(1): 265–275.
35. Wilbur KM & Anderson NG (1948). Electrometric and colorimetric determination of carbonic anhydrase. Journal of Biological Chemistry, 176(1): 147–154.
36. Andersson I & Backlund A (2008). Structure and function of Rubisco. Plant Physiology and Biochemistry, 46(3): 275–291.
37. Vidal J & Chollet R (1997). Regulatory phosphorylation of C_4 PEP carboxylase. Trends in Plant Science, 2(6): 230–237.
38. Zelitch I & Ochoa S (1953). Oxidation and reduction of glycolic and glyoxylic acids in plants. Journal of Biological Chemistry, 201(2): 707–718.
39. Aebi H (1984). Catalase in vitro. Methods in Enzymology, 105: 121–126.
40. R Core Team (2023). R: A Language and Environment for Statistical Computing. R Foundation for Statistical Computing, Vienna, Austria.